Journal of the Serbian Chemical Society
JSCS-info@shd.org.rs • www.shd.org.rs/JSCS

ACCEPTED MANUSCRIPT

This is an early electronic version of an as-received manuscript that has been accepted for publication in the Journal of the Serbian Chemical Society but has not yet been subjected to the editing process and publishing procedure applied by the JSCS Editorial Office.

Please cite this article as M. M. Helmy and A. S. El Mahrouky, *J. Serb. Chem. Soc.* (2026) https://doi.org/10.2298/JSC260123069H

This "raw" version of the manuscript is being provided to the authors and readers for their technical service. It must be stressed that the manuscript still has to be subjected to copyediting, typesetting, English grammar and syntax corrections, professional editing and authors' review of the galley proof before it is published in its final form. Please note that during these publishing processes, many errors may emerge which could affect the final content of the manuscript and all legal disclaimers applied according to the policies of the Journal.

Journal of the Serbian Chemical Society
JSCS-info@shd.org.rs • www.shd.org.rs/JSCS
J. Serb. Chem. Soc. **00(0)** 1-28 (2026)
JSCS–13742
Original scientific paper
Published DD MM, 2026

Accepted manuscript

Sustainable remediation of olive mill wastewater: Comparison of phenolic compound removal using rice husk-derived nanosilica and sodium silicate

MARWA M. HELMY* AND AMIRA S. EL MAHROUKY

Food Engineering and Packaging Department, Food Technology Research Institute, Agricultural Research Center, Giza, Egypt.

(Received 23 January; revised 3 March; accepted 13 November 2026)

Abstract: This study investigates the remediation of olive mill wastewater (OMW) using nanosilica and sodium silicate extracted from rice husk. Characterized by FTIR, UV-Visible spectroscopy, and particle size analysis, these sustainable adsorbents were evaluated for the removal of phenolic compounds. Response Surface Methodology (RSM) was employed to optimize batch adsorption parameters, including concentration, mixing time, and rotational speed. Nanosilica demonstrated superior performance, achieving a maximum adsorption capacity of 1024.9 mg/g and 89.979% removal efficiency under optimal conditions (0.5% concentration, 15 min, 200 rpm). In comparison, sodium silicate yielded a capacity of 130.68 mg/g and 72.45% removal (2% concentration, 52.5 min, 300 rpm). Furthermore, kinetic and isotherm models were applied to describe the adsorption mechanisms. Mechanistic investigations utilizing the Weber-Morris model established that adsorption is controlled by a multi-step sequence of film and intra-particle diffusion, with nanosilica demonstrating a remarkably higher intra-particle diffusion rate (Kid = 18.879 mg $g^{-1}min^{-0.5}$). Furthermore, thermodynamic parameters ($\Delta G < 0$) and the Dubinin–Radushkevich isotherm (E < 8 kJ/mol) conclusively proved that the sequestration process is governed by spontaneous physisorption. These findings confirm the potential of rice husk-derived materials as efficient, eco-friendly adsorbents for OMW treatment.

Keywords: response surface methodology; FTIR; adsorption; kinetic models; isotherm models.

INTRODUCTION

The growing scarcity of freshwater resources has significantly increased the demand for efficient wastewater treatment technologies. The reuse and recycling

* Corresponding author. E-mail: marwahelmy81@yahoo.com
https://doi.org/10.2298/JSC260123069H

of wastewater are crucial for mitigating water scarcity, protecting ecosystems, and achieving sustainable development.[1]

The olive oil industry is a significant polluter, generating substantial amounts of wastewater known as olive mill wastewater (OMW) rated at approximately 30 million m^3 annually, alongside about 20 million tons per year of solid waste (pomace).[2] OMW is ranked among the most polluting effluents from the agro-food sector, contributing to resource depletion, soil deterioration, and air pollution.[3] It is characterized by a strong odor, dark color, low pH (typically between 3 and 6), and a very high organic load.[4] This is reflected in high levels of Chemical Oxygen Demand (COD) and Biochemical Oxygen Demand (BOD), as well as high concentrations of total suspended solids (TSS), total dissolved solids (TDS), and phenolic compounds.[5]

Among its most hazardous pollutants are polyphenolic components (such as tannins, flavanols, and anthocyanins), with concentrations ranging from 0.1 to 18 g/L.[6] These compounds not only contribute to the high toxicity and biorecalcitrance of OMW, limiting the effectiveness of biological treatment, but their discharge without adequate remediation also leads to severe environmental and health problems. These include the contamination of surface and groundwater, and the endangerment of aquatic ecosystems.[4]

Given the complex characteristics of OMW, conventional single-unit treatment methods—whether physical, chemical, or biological—often prove insufficient as standalone solutions or are economically impractical.[4] Consequently, recent research has emphasized combined treatment processes that leverage the synergy of multiple technologies to achieve high removal efficiencies of up to 85–90%.[7]

Coagulation and Flocculation (CF) are among the oldest and most widely employed preliminary treatment techniques due to their simplicity, cost-effectiveness, and low energy demand. In line with the global shift towards sustainability, there is growing interest in using natural coagulants as alternatives to traditional chemical-based ones, owing to their greater biodegradability, lower toxicity, reduced cost, and lower sludge production.[8]

Within this framework, the valorization of agricultural waste as a raw material for treatment agents presents a promising approach. Rice husk is a prominent agricultural residue, and its combustion yields Rice Husk Ash (RHA), which is rich in silica (SiO_2) with content ranging from 90% to 98%.[9] This ash can be chemically treated (e.g., via acid leaching) to remove metallic impurities and produce high-purity silica. Rice husk-derived silica, particularly in its nano form (nanosilica), possesses exceptional properties that make it an effective adsorbent. These include a very high surface area to volume ratio, excellent stability, and low toxicity, enabling the removal of specific pollutants like phenols and heavy metals from water.[10]

Accepted manuscript

Furthermore, RHA can serve as a sustainable precursor for the production of sodium silicate (commonly known as water glass), which is a fundamental intermediate in various industrial and chemical applications. This integrated approach represents a circular economy model, transforming an agricultural waste (rice husk) into valuable materials (nanosilica and sodium silicate), which are in turn used to treat another hazardous waste stream (OWM).[3]

Despite the severe environmental impact of olive mill wastewater (OMW) primarily driven by its high concentration of phytotoxic and recalcitrant phenolic compounds developing cost-effective, highly efficient, and sustainable treatment technologies remains a significant global challenge. While adsorption is widely acknowledged as a promising remediation strategy, conventional commercial adsorbents are often prohibitively expensive and environmentally taxing to manufacture. Consequently, recent literature has shifted toward circular economy approaches; however, a critical knowledge gap persists regarding the targeted valorization of abundant agricultural byproducts into high-value nanoscale adsorbents specifically engineered for OMW remediation.

The primary objective of this research is to evaluate the effectiveness of rice husk-derived nanosilica and sodium silicate as adsorbents for treating olive mill wastewater (OMW). This will be achieved through the following specific aims:

- Synthesis: To extract and synthesize nanosilica and sodium silicate from rice husks, utilizing a sustainable and readily available agricultural byproduct.
- Optimization: To optimize the treatment process using Response Surface Methodology (RSM), determining the ideal adsorbent concentration, contact time, and rotational speed required to maximize the removal of phenolic compounds.
- Mechanistic Analysis: To investigate the underlying adsorption mechanisms by applying various isotherm and kinetic models to the experimental data, thereby gaining a deeper theoretical understanding of the treatment process.

MATERIALS AND METHODS

Materials

Rice husk (RH) was obtained from a local rice mill company in Dimitta, Egypt. A solution of 35% hydrochloric acid (HCl, Merck, India) was used to remove mineral impurities from the rice husk. Other chemicals, including sodium hydroxide (NaOH, reagent grade ≥ 98%, anhydrous pellets), hydrochloric acid (HCl, ACS reagent, 37%), gallic acid (ACS reagent ≥ 97.5%), Folin & Ciocalteu's reagent (Sigma-Aldrich, France), Sodium bicarbonate (Sigma-Aldrich, France), ethanol, and distilled water, were used as needed. An olive mill wastewater (OMW) sample was collected from an olive oil extraction unit at the Food Technology Research Institute (Egypt). The sample was stored at 4 °C to avoid the oxidation and subsequent polymerization of phenolic compounds.

Accepted manuscript

Characterization of raw OMW

The physiochemical properties of the olive mill wastewater (OMW) were characterized using standard methods. Biological Oxygen demand (BOD) was measured using (WTW, Germany) incubator system. Chemical Oxygen demand (COD) was determined with a photolab and WTW reactor, while turbidity was analyzed using a WTW turbidity meter. Dissolved oxygen and pH were measured with an EZODO pH 5011 meter. The concentrations of total nitrogen, iron (Fe), and copper (Cu) were quantified using a WTW spectrophotometer.

Synthesis of sodium silicate

Sodium silicate was synthesized from rice husk (RH) using a modified alkaline extraction method, Fig. 1. First, 50 g of ground RH was incinerated in a muffle furnace at 700°C for two hours to produce rice husk ash (RHA). The RHA was then mixed with a 1 M NaOH solution and heated to 100 °C for 2 hours under constant stirring to dissolve the silica. The mixture was filtered, and the filtrate was concentrated to two-thirds of its original volume. Crystallization was initiated by seeding the concentrate with pure sodium silicate crystals. The product crystals were isolated by decanting the supernatant, washed with cold distilled water, and finally stored in a polyethylene container.[11]

Synthesis of nanosilica

Nanosilica was synthesized from the sodium silicate solution using a precipitation method, Fig. 2. Concentrated HCl was added dropwise to the vigorously stirred sodium silicate solution to lower the pH, inducing the formation of a silica gel. This gel was then dried in an electric furnace at 200°C for eight hours. The resulting solid was ground into a fine powder and subsequently stored in a desiccator for further characterization.[9,12]

$$SiO_2 + 2NaOH \rightarrow Na_2SiO_3 + H_2O$$
$$Na_2SiO_3 + 2HCl \rightarrow SiO_2 + 2NaCl + H_2O$$

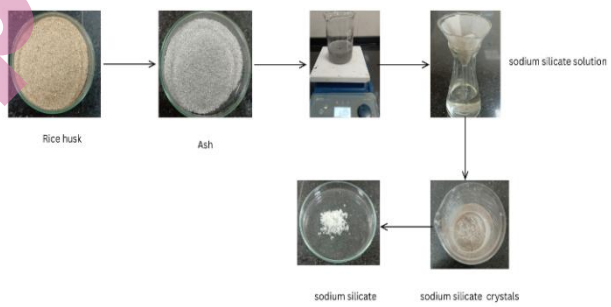


Fig.1. The synthesis of sodium silicate.

Accepted manuscript

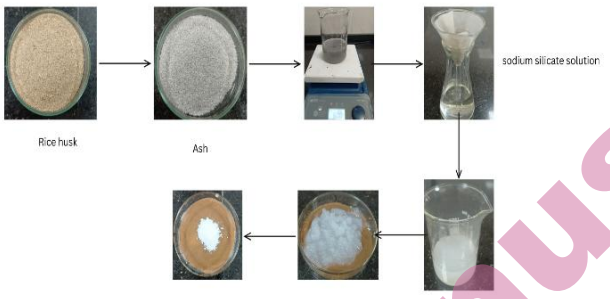


Fig.2. The synthesis of nanosilica.

Characterization of adsorbents

The synthesized adsorbents were characterized using Fourier-Transform Infrared (FTIR) spectroscopy, UV-Visible spectroscopy, and particle size analysis. Functional groups were identified by FTIR spectroscopy (Bruker Invenio S, Germany) over a wavenumber range of 4000 to 400 cm^{-1}. Optical properties were assessed with a T90 Double Beam Spectrophotometer (PG Instruments Ltd) by measuring optical absorption across wavelength range of 200 to 800 nm. The powder was milled, and the particle size distribution was determined using laser diffraction analysis (Malvern Instruments Ltd). The different adsorbents were analyzed for morphological features using a scanning electron microscope SEM (Quanta 250 FEG, Netherlands).

Adsorption process

Laboratory-scale batch adsorption tests were performed using a six-station jar test apparatus to evaluate the efficacy of two adsorbents: nanosilica and sodium silicate. The experimental design systematically varied three key parameters: stirring speed (100, 200, and 300 rpm), contact time (15, 52.5, and 90 minutes), and adsorbent concentration. The concentrations used were 0.5, 1, and 2% for nanosilica, and 1, 2, and 4% for sodium silicate. Following adsorption and subsequent centrifugation at 4000 rpm for 20 min, the supernatant was carefully siphoned for further analysis.

pH measurment

The pH samples was measured using a pH meter (EZODO pH 5011). The point of zero charge (pHpzc) for the adsorbents was determined using the salt addition method, with a solution of NaCl (0.01 mol/L) as background electrolyte. This background solution was placed in 6 flasks (50 mL in each) increasing the pH values in each flask (2–12). This procedure was performed for every solid, adding 0.1 g and determining the change in the pH of each solution after shaking the capped samples at 150 rpm for 48 h at 24 ºC. The pH change observed was plotted against the initial pH values, thereby determining the pHpzc, which is the pH when ΔpH = 0.[12]

Analysis of total phenolic compounds

The phenolic fraction of olive mill wastewater (OMW) is highly complex, predominantly comprising simple phenolic alcohols, phenolic acids, and flavonoids. The most abundant and representative chemical forms responsible for its high toxicity are hydroxytyrosol ($C_8H_{10}O_3$; 4-(2-hydroxyethyl)-1,2-benzenediol) and tyrosol $C_8H_{10}O_2$; 4-(2-hydroxyethyl)phenol). In this

Accepted manuscript

study, gallic acid $C_8H_{10}O_5$; 3,4,5-trihydroxybenzoic acid) was utilized as the standard chemical reference for the quantification of total phenolic compounds. The molecular structures of these primary representative phenolics are illustrated in Fig. 3.

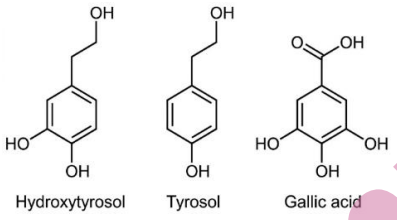


Fig.3. Chemical structures of the predominant phenolic compounds in olive mill wastewater (hydroxytyrosol and tyrosol) and the reference standard used for quantification (gallic acid).

The total phenolic compounds were analyzed by UV-visible spectrophotometry at 760nm.[16] A calibration curve was established using a series of gallic acid solutions (50, 100, 200, 300, 400, and 500 mg/L). The measurements were conducted as follows: aliquot of the gallic acid solution (100 µL) were mixed with 6 mL of distilled water, 500 µL of Folin & Ciocalteu's reagent, and 1.5 mL of a Na_2CO_3 solution. The mixtures were then diluted to a final volume 10 mL with distilled water, incubated for 2 h, and stirred vigorously before measurement.[13]

For the treated olive mill wastewater, the adsorption capacity, qe (mg/g), and the adsorption yield (%) were calculated using the following equations:

$$q_e = \frac{(c_o - c_e)V}{W} \quad (1)$$

$$Adsorption\ yield(\%) = \frac{(c_o - c_e)}{c_o} * 100 \quad (2)$$

Where, Co and C_e (mg/L) are the initial and equilibrium concentrations of phenolic compounds respectively. V (L) is the volume of the solution, and W (g) dry mass of adsorbent.

Isotherm models

The adsorption equilibrium data were evaluated using the Langmuir and Freundlish isotherm models, represented by equations (3) and (4). The Langmuir isotherm model describes a monolayer adsorption process on a homogeneous surface. The key parameters obtained from this model are q_e (the amount of adsorbate adsorbed at equilibrium). C_e (the equilibrium concentration of phenolic compounds in solution), KL (the Langmuir constant related to the adsorption energy), and q_m (the maximum adsorption capacity of phenolic compounds).[14]

$$\frac{c_e}{q_e} = \frac{1}{KL \times qm} + \frac{c_e}{qm} \quad (3)$$

The Freundlich isotherm model, expressed by Equation (4), describes multilayer adsorption on a heterogeneous surface. This model involves two empirical constant *Kf* and n, which represent the adsorption capacity of the adsorbent and the intensity of the adsorption process, respectively.[14]

$$log\ q_e = log\ K\ f + \frac{1}{n} log\ c_e \quad (4)$$

Accepted manuscript

The Dubinin–Radushkevich (D–R) model took into account the Gaussian energy distribution on the heterogeneous surface of the adsorbent, which could identify the nature of adsorption.[15] The linearized form was defined by Eq. (5).

$$ln\,q\,e = ln\,q\,m - \beta.\varepsilon^2 \quad (5)$$

Where β (mol^2/kJ^2) is a constant related to the mean free energy change, ε is the Polanyi potential and could be determined by Eq. (6). The mean free energy (kJ/mol) could be calculated using Eq. (6 and 7)

$$\varepsilon = RT\,ln(1 + \frac{1}{C_e}) \quad (6)$$

$$E = \frac{1}{\sqrt{2\beta}} \quad (7)$$

Where R (8.314 J/mol/K) is the ideal gas constant and T (K) is the absolute temperature.

Kinetic models

To investigate the removal kinetics of phenolic compounds, two kinetic models were applied: the pseudo first order and pseudo second order rate equations. These models, presented in equations (8) and (9), were used to elucidate the adsorption mechanisms and rate-controlling steps. The kinetic parameters obtained from these models include q_e and q_t (the amount of phenolic compounds adsorbed at equilibrium and at time t respectevily), as well as k_1 and k_2 (the rate constant for the pseudo first order and pseudo second order models, respectively).[16]

$$log(q_e - q_t) = log\,q_e - \frac{K1}{2.303}t \quad (8)$$

$$\frac{t}{q_t} = \frac{1}{K2 \times q_e^2} + \frac{t}{q_e} \quad (9)$$

To evaluate the rate-limiting mechanisms and assess the influence of boundary layer resistance, the data were analyzed using the Weber–Morris intra-particle diffusion model (Eq. 10). This model is defined as

$$qt = Ki.t^{0.5} + C \quad (10)$$

Where Kid (mg/g $min^{0.5}$) is the intra-particle diffusion rate constant, and C is usually related to the boundary layer thickness.[17]

Thermodynamic parameters

The thermodynamic parameters, including the standard enthalpy change (ΔH◦) and standard entropy change (ΔSº), were determined from the slope and intercept of the linear plot of the Van't Hoff equation (ln (Kc) vs.1/T), using equilibrium adsorption data obtained at different temperatures (35,45 and 55 ºC). The standard Gibbs free energy change (ΔG◦) at each temperature was subsequently calculated using Eq. (11-14).[18]

$$Kc = \frac{co - ce}{co} \quad (11)$$

$$\Delta G° = -R.T.ln\,K\,c \quad (12)$$

$$\Delta G° = \Delta H° - T.\Delta S° \quad (13)$$

$$LnKc = \frac{\Delta S°}{R} - \frac{\Delta H°}{RT} \quad (14)$$

Where C0 and Ce are the initial concentration and equilibrium concentration, R is the universal gas constant (8.314 $J.mol^{-1}.K^{-1}$), and T is the absolute temperature (K).

Accepted manuscript

Statistical analysis

Response surface methodology (RSM) was utilized in the experiments, utilizing a Box-Behnken design (BBD) to optimize the removal of phenolic compounds. This approach involved selecting three independent variables: rotational speed (X_1), mixing time (X_2), and adsorbent concentration (X_3). The range for each variable was chosen based on preliminary batch adsorption experiments: rotational speed at 100, 200, and 300 rpm; mixing time at 15, 52.5, and 90 minutes; and adsorbent concentration at 0.5, 1, and 2% for nanosilica, or 1, 2, and 4% for sodium silicate. The percentage removal of phenolic compounds was defined as the response variable. Model fitting, statistical evaluation, and optimization of the operating conditions were conducted using Design Expert 13.0 statistical software by solving the generated regression models.[19]

RESULTS AND DISCUSSION

Adsorbents characterization

The FTIR of sodium silicate and nanosilica characterization

Fourier-transform infrared (FTIR) was utilized to elucidate the surface chemistry and primary adsorption mechanisms of the synthesized nanosilica and sodium silicate before and after exposure to olive mill wastewater (OMW). The FTIR spectra of the nanosilica and sodium silicate samples are presented in fig. 4. For the nanosilica spectrum (Fig. 4a), the dominant absorbance peak at 1068 cm^{-1} corresponds to the asymmetric stretching vibration of Si-O-Si bonds. The peaks at 797 cm^{-1} and 460 cm^{-1} are attributed to the symmetric stretching and bending vibrations of siloxane bonds Si-O-Si, respectively. A broad band at 3410 cm^{-1} is associated with O–H stretching from adsorbed water, while the peak at 1632 cm^{-1} represents H–O–H bending vibrations.[19]

After exposure to OMW (Fig. 3b), the preservation of characteristic Si–O–Si bands (1081.98, 793.05, and 458.43 cm^{-1}) confirms that the silica matrix remains intact during treatment without bulk structural degradation. The near complete disappearance of the broad O–H band (3413.69 cm^{-1}) and emergence of isolated silanol peaks indicate that surface Si–OH groups serve as the primary active sites via hydrogen bonding and dipole–dipole interactions[20]. The appeareance of a new phenolic-associated band at 1319.59 cm^{-1} (C–O / O–H vibration) and the shift in Si–OH stretching to 956.64 cm^{-1} provide direct spectroscopic evidence of successful surface complexation and phenolic immobilization.

Figure 4c displays the FTIR spectrum of sodium silicate, which showed characteristic bands including a broad peak at 3346 cm^{-1}, at attributed to –OH group stretching associated with moisture. The peaks at 1664 and 1754 cm^{-1} also correspond to vibrations of water molecules.[20] Peaks observed at 991, 914, and 817 cm^{-1} are assigned to Si–O stretching within the silicon tetrahedron.[21] Additionally, the bands at 1441 and 1468 cm^{-1} are attributed to the symmetric C–O stretching of C-O-Si groups, likely due to trace carbon or CO_2 absorption during synthesis. The peak around 2559 cm^{-1} may be associated with O=C=O stretching, indicating

Accepted manuscript

possible exposure of the sodium silicate crystals to atmospheric carbon dioxide during the draining process.[22]

Figure 4d illustrated spectrum of sodium silicate after exposure to OMW, spectrum reveals the emergence of several distinct new bands in the 1400–1600 cm^{-1} region specifically at 1593.15, 1541.09, and 1488.54 cm^{-1} along with a new peak at 1229.33 cm^{-1}. These signals are highly characteristic of aromatic ring vibrations (C=C) and carbon-oxygen (C–O) stretching from the adsorbed organic molecules, confirming the successful immobilization of the adsorbate onto the sodium silicate surface. Despite these substantial surface modifications, the fundamental structural integrity of the adsorbent is maintained, as evidenced by the preservation of the characteristic siloxane (Si–O–Si) asymmetric stretching band, which undergoes only a negligible shift from 1083.56 cm^{-1} to 1086.69 cm^{-1}. These combined spectroscopic findings indicate a robust surface complexation mechanism driven by the interaction between the adsorbate and the surface hydroxyls of the stable silicate framework.

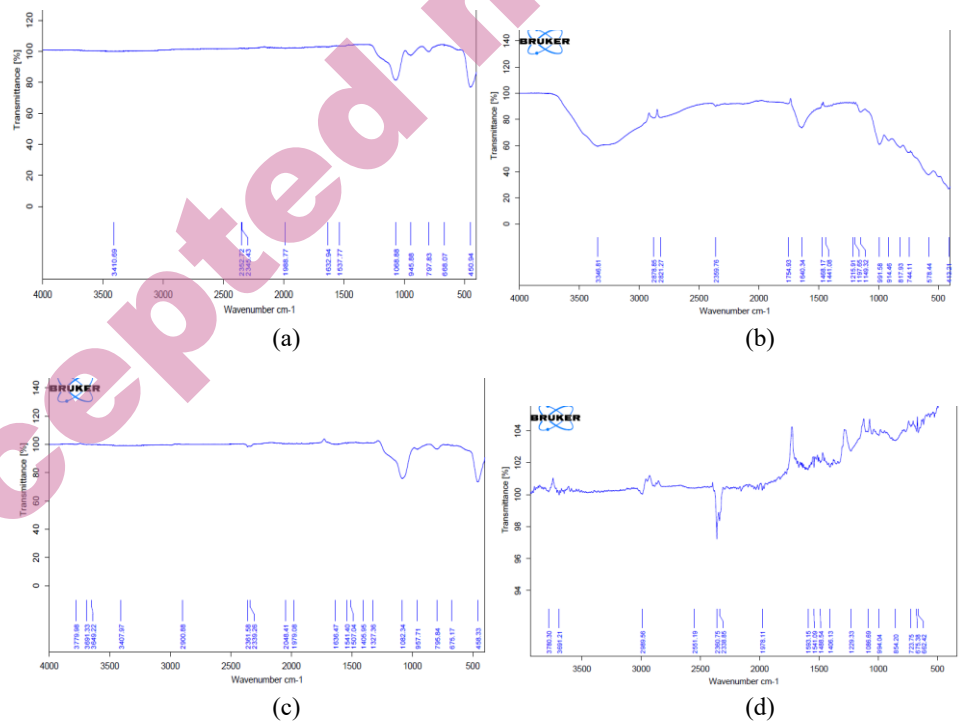


Fig. 4. FTIR for (a) nanosilica before adsorption, (b) nanosilica after adsorption, (c) sodium silicate before adsorption and (d) sodium silicate after adsorption.

Accepted manuscript

Size distribution of adsorbents

The hydrodynamic diameter of the synthesized nanoparticles was determined by dynamic light scattering (DSL). The number-weight size distribution revealed a monomodal population with mean diameters of 21.04 ± 9.06 nm for nanosilica and 220 ± 14.82 nm for sodium silicate (Fig. 5). The polydispersity index (PDI) values of 0.493 and 0.557 for nanosilica and sodium silicate, respectively, indicate a moderately broad size distribution, which is characteristic of the chosen synthesis route. The nanometric size of the nanosilica is consistent with the formation of a colloidal suspension and suggests a high specific surface area, which is advantageous for the adsorption of phenolic compounds.[10]

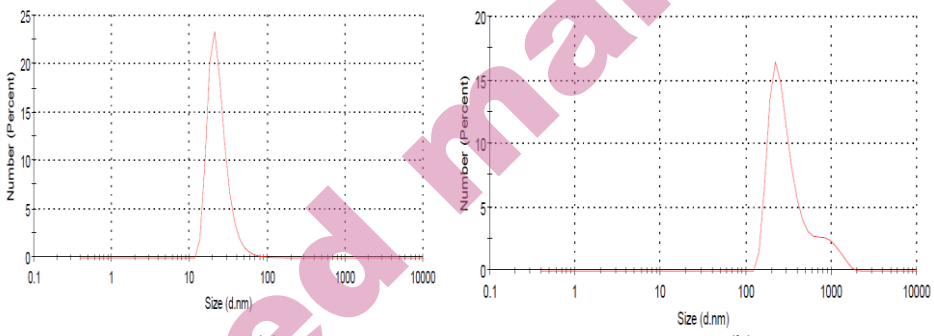


Fig. 5. Particle size of adsorbents, (a) nanosilica, (b) sodium silicate.

UV-Visible spectroscopy

Ultraviolet-visible spectroscopy was used to explore the optical properties of the synthesized particle. Absorption spectra were recorded over a spectral range of 250 to 500 nm, plotting optical absorbance as a function of wavelength (Fig. 6). Both nanosilica and sodium silicate exhibited strong adsorption in the UV region, with maximum absorbance observed at 259 and 263 nm, respectively. The results confirm the successful formation silicon dioxide nanoparticles. The absorption in this region is attributed to electronic transitions within the molecules or lattice structures; absorption extending into the visible range directly influences the material's perceived color.[23]

Accepted manuscript

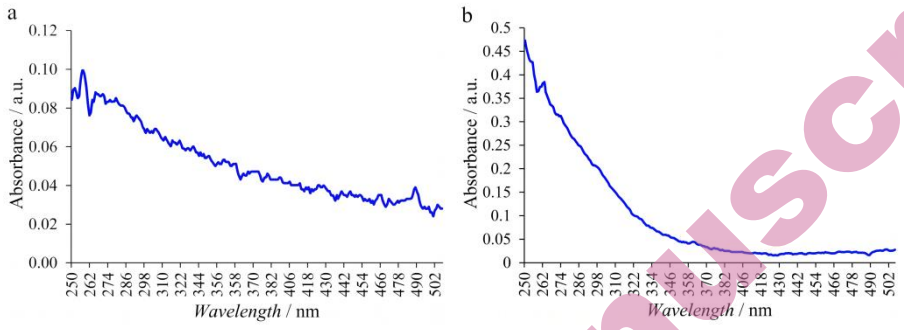
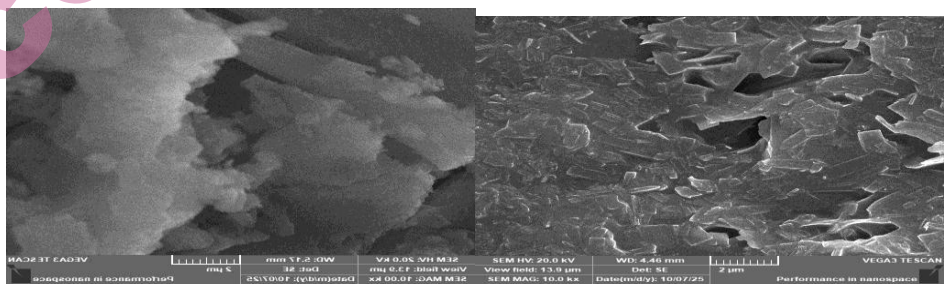


Fig.6. UV-Visible spectra (a) nanosilica and (b) sodium silicate.

Scanning electron microscopy (SEM)

Comparative analysis of the scanning electron microscopy SEM in Fig. 7 reveals a significant morphological and structural disparity between sodium silicate and nanosilica. Sodium silicate exhibits a micro-scale structure consistent with a crystalline form, characterized by angular, platy particles with defined facets and clear intercrystalline boundaries. This morphology contrasts sharply with that of nanosilica, which displays a highly globular and aggregated texture typical of amorphous silica (SiO_2).[24] The clustered nature of nanosilica results from the high surface energy of primary nanoparticles, driving agglomeration into larger masses and creating a highly porous internal structure. This morphological contrast dictates their functional efficacy in contaminant removal. While the dense crystalline structure of sodium silicate renders it generally unsuitable for direct adsorption due to low surface area, the amorphous nanosilica is highly effective. The extensive clustering in nanosilica directly results from its high surface area and mesoporosity, which maximize the available active sites for binding contaminants such as heavy metals and organic dyes.[25]



(a) (b)

Fig.7. Scanning Electron Microscopy SEM micrographs for a. nanosilica and b. sodium silicate.

Accepted manuscript

Characterization of raw OMW

The physiochemical properties of the raw olive mill wastewater are summarized in Table I. The OMW was notably acidic (pH 5.1), which is attributed to the presence of the organic acids such as phenolic compounds.[26] A high turbidity of 780 NTU was measured, resulting from suspended particles, including colloidal matter. The wastewater exhibited a high organic load, with chemical oxygen demand COD and biochemical oxygen demand BOD values measured at 230.4 g/L and 14.1 g/L respectevily, which is consistent with findings from other studies. The concentrations of metals and total nitrogen were determined as follows: iron (Fe) at 93 ppm, copper (Cu) at 202 ppm, and total nitrogen (ΣN) at 445 ppm. The concentration of polyphenols in the raw OMW was 15.8 g/L. Importantly the polyphenol content in OMW depends on factors such as olive fruit variety, maturity, climatic conditions, and the specific technological processes used for oil extraction.[27]

Table I: The physicochemical properties of olive mill wastewater OMW.

parameters	pH	Turbidity (NTU)	Polyphenols (g/L)	Fe (ppm)	Cu (ppm)	ΣN (ppm)	COD (g/L)	BOD (g/L)
values	5.1	780	15.8	93	202	445	230.4	14.1

Factorial design experiment

The experimental conditions and the corresponding phenolic compound removal percentages for both adsorbents, nanosilica and sodium silicate was presented in Table II. The data show that phenolic removal ranged from 85% to 89.97% for nanosilica and from 43.25% to 72.45% for sodium silicate. Regression analysis was generated to fit response function to the experimental data, determining the major effects of the factors (rpm, time, and concentration) as well as their interaction effects. The model equation is expressed in terms coded factors for nanosilica as an adsorbent is as follows:

$$\text{Phenolic compounds removal} = 89.0273 + 0.446315A - 0.855963B + 0.641113\,C + 1.09889\,AB - 0.0847942\,AC - 0.475535BC - 0.974872A^2 - 0.577256B^2 - 0.45694\,C^2 \quad (15)$$

The model equation is expressed in terms coded factors for using sodium silicate as adsorbent was described as follows:

$$\text{Phenolic compounds removal} = 45.0431 - 4.14163\,A - 0.224375\,B + 7.87825\,C + 0.51275\,AB - 3.388\,AC + 1.569\,BC + 3.72433\,A^2 + 3.03283\,B^2 + 8.91007\,C^2 \quad (16)$$

The analysis of variance (ANOVA) for the model fitted to the nanosilica adsorption data is presented in Table III. The model revealed a statistically significant and robust relation between the independent variables and the response. The high F-value (15.31) and low p-value <0.0001 confirm the model's statistical

Accepted manuscript

significance and its effectiveness in explaining the data variation. All three main factors (A: rpm, B: time, C: concentration) were significant linear contributors. The analysis also indicated significant nonlinear behavior, as shown by the significant quadratic terms (A^2, B^2, C^2). Regarding interaction effects, the AB (rpm × time) interaction was significant, the AC (rpm × concentration) interaction was not significant, and the BC (time × concentration) interaction was marginally non-significant.

The ANOVA results for the sodium silicate model are shown in Table IV. This model was also highly effective, with a significant F-value of 64.57 ($p < 0.0001$), powerfully explaining the variation in the data. Concentration (C) and rotational speed (A) were the most influential factors, exhibiting significant effects both as linear and quadratic terms. A significant interaction was also found between rpm and concentration (AC). In contrast, mixing time (B) had no significant linear effect. Furthermore, the non-significant lack-of-fit test ($p = 0.2010$) confirms that the model fits the data well, establishing its reliability for prediction and optimization.

Table II: the experimental design matrix and experimental resuls.

Run	rpm	Time (min)	Concentration (%)		phenolic removal (%)		pH	
	A	B	nanosilica	Sodium silicate	nanosilica	Sodium silicate	nanosilica	Sodium silicate
1	200	15	2.0	4.0	89.552	47.086	7.6	11.6
2	200	52.5	1.0	2.0	88.979	43.250	7.4	12.3
3	100	52.5	0.5	1.0	86.083	44.120	6.9	11.4
4	100	90.0	1.0	2.0	85.001	45.030	7.5	12.2
5	100	52.5	2.0	4.0	88.296	55.489	8.0	12.4
6	200	15.0	0.5	2.0	89.979	49.681	7.4	12.3
7	200	52.5	1.0	2.0	88.979	43.880	7.1	12.3
8	200	52.5	1.0	2.0	88.979	44.100	7.3	12.3
9	300	52.5	1.0	2.0	87.751	72.450	7.5	12.4
10	200	52.5	1.0	2.0	88.979	48.254	7.1	12.3
11	200	52.5	1.0	2.0	88.797	46.120	7.4	12.3
12	300	90.0	1.0	2.0	88.173	58.254	7.6	12.3
13	200	90.0	2.0	4.0	86.953	47.010	7.8	12.4
14	100	15.0	1.0	2.0	88.975	45.550	7.7	12.3
15	200	52.5	1.0	2.0	88.597	49.329	7.4	12.3
16	300	15.0	0.5	1.0	88.081	59.250	6.7	11.6
17	200	52.5	1.0	2.0	89.000	46.372	7.1	12.3
18	200	52.5	1.0	2.0	89.001	62.580	7.4	12.3
19	300	52.5	0.5	1.0	87.063	47.251	6.9	11.5
20	200	90.0	0.5	1.0	87.384	50.550	6.7	11.5
21	300	52.5	2.0	4.0	88.938	44.120	8.0	12.5
22	200	52.5	1.0	2.0	88.979	66.560	7.4	12.3

Accepted manuscript

Table III: Analysis of variance ANOVA for the phenolic removal by nanosilica .

					0.0015
A^2	4.47	1	4.47	22.93	0.0004
B^2	1.57	1	1.57	8.04	0.0150
C^2	0.9826	1	0.9826	5.04	0.0444
Residual	2.34	12	0.1951		
Lack of Fit	1.18	3	0.3943	3.06	0.0839
Pure Error	1.16	9	0.1287		
Cor Total	29.22	21			

Table IV: Analysis of variance ANOVA for the phenolic removal by sodium silicate.

					< 0.0001
AB	1.05	1	1.05	0.4466	0.5166
AC	45.91	1	45.91	19.50	0.0008
BC	9.85	1	9.85	4.18	0.0634
A^2	65.27	1	65.27	27.72	0.0002
B^2	43.28	1	43.28	18.38	0.0011
C^2	373.60	1	373.60	158.64	< 0.0001
Residual	28.26	12	2.36		
Lack of Fit	10.94	3	3.65	1.89	0.2010
Pure Error	17.32	9	1.92		
Cor Total	1396.84	21			

Effect of adsorbents on OMW pH

The point of zero charge (pHpzc) of the synthesized adsorbents was determined using the pH drift method to evaluate their surface charge characteristics in aqueous solutions. As depicted in Figure 8, the curves intersected the horizontal axis (Δ pH = 0) at distinct points for each material. The pHpzc value for the rice husk-derived nanosilica was found to be 4.0, whereas for the sodium silicate, it was recorded at 2.4. These results indicate that the surfaces of both nanosilica and sodium silicate are predominantly acidic. Specifically, their surfaces acquire a net positive charge at pH levels below their respective pHpzc

Accepted manuscript

values and a net negative charge at higher pH levels, primarily due to the deprotonation of surface silanol groups (Si-OH → Si-O$^-$). This surface charge behavior plays a vital role in facilitating the electrostatic interactions and hydrogen bonding with the phenolic compounds during the treatment of the olive mill wastewater.[12]

The pH is widely recognized as a critical parameter in the adsorption process, as it governs both the ionization state of phenolic compounds and the surface charge of the nanosilica and sodium silicate adsorbents. Table II shows the variation in the pH of olive mill wastewater (OMW) following the addition of different concentrations of these adsorbents. The influence of pH further differentiates the two adsorbents. Nanosilica operated most effectively under neutral to slightly alkaline conditions (pH 6.7–8.0), where phenolic compounds are partially deprotonated, enhancing their adsorption onto the silica surface. Sodium silicate, however, required a highly alkaline environment (pH 11.4–12.5) for optimal performance. At such extreme pH levels, phenolic compounds fully deprotonate into phenolate ions, but the abundance of hydroxide ions (OH^-) may compete for adsorption sites, potentially reducing overall efficiency. This limitation makes sodium silicate less practical for industrial applications where pH adjustment to such extremes is undesirable.[28] The observed adsorption behavior is consistent with findings from a range of studies using diverse adsorbents, including sugarcane bagasse, oregano-modified bentonite, pomegranate seeds and commercial activated carbon.[29] These studies generally report increased adsorption of phenolic compounds decreased pH levels and a decline at increased pH values, although some contrasting results exist. Such variations can be assigned to the interplay between the adsorbent surface charge and the pHpzc of the specific phenolic compounds present in OMW. It is well established that the phenolic molecule residue largely undissociated when the pH solution is below their pHpzc, while at pH values above the pHpzc, they dissociate into negatively charged anions.[14]

Accepted manuscript

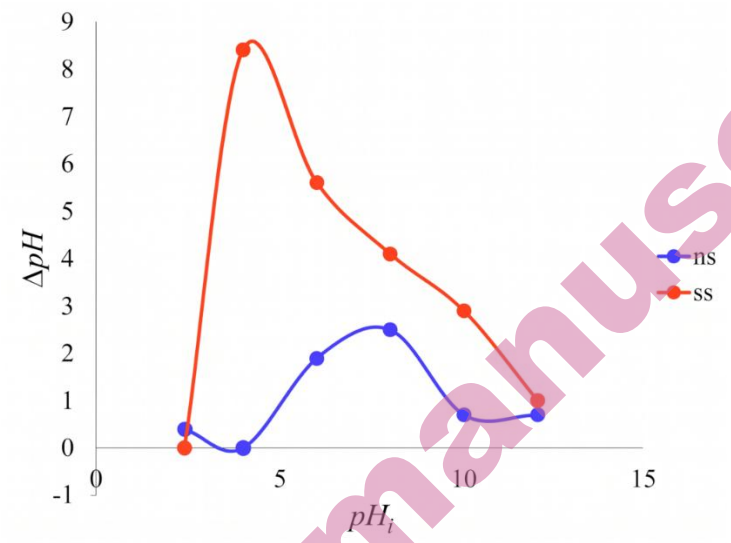


Fig. 8. The point zero charge pH (pHpzc) of nanosilica and sodium silicate.

Effect of adsorption conditions on removal of phenolic compounds

Effect of adsorbent dosage

Figure 9 illustrates the response surface 3D plots, rendering the interactions between independent variables and their effect on phenolic compound removal. For nanosilica, when the adsorbent mass was risen from 0.5% to 2%, the adsorption capacity for phenols increased from 252.95 to 1024.9 mg/g, corresponding to a removal percentage of 85% to 89.55%. In contrast, for sodium silicate with a mass ranging from 1% to 4%, the adsorption capacity ranged from 30.75 to 130.68 mg/g, corresponding to a removal percentage of 43.25% to 72.45%.

Additional active sites, which are provided for pollutant binding, cause the initial decrease in the removal efficiency with adsorbent dosage. However, beyond a nanosilica dosage of 0.5%, the adsorption capacity exhibited a marginal decline in spite of the increase in adsorbent mass. This plateauing or slight decrease can be attributed to the saturation of pollutants in the solution, leading to suboptimal utilization of the available active sites and a consequent reduction in adsorption efficiency per unit mass. Furthermore, at adsorbent concentrations exceeding 1%, particle agglomeration may occur, the effective surface area is diminished and active site is blocking, thereby moreover impeding the adsorption process.[30] The optimal adsorbent dosage was determined to be approximately 0.5% for nanosilica and 2% for sodium silicate, as these quantities maximize adsorption capacity while maintaining an efficient balance between pollutant removal and adsorbent utilization.[31]

Accepted manuscript

According to the literature, increasing the adsorbent dosage beyond the optimum level typically reduce the amount of phenol adsorbed per unit of adsorbent weight.[14] For instance, Ververi & Goula.[32] attributed a similar decline in phenolic compound adsorption on wheat bran at higher dosages to particle agglomeration reducing the available surface area. However, the findings of the present study show a different trend, where the adsorption capacity for nanosilica increased significantly with dosage. This deviation from established observations may be explained by the high initial pollutant load and the initiation of a new equilibrium between adsorbed and non-adsorbed phenolic compounds in the solution.

Effect of contact time the adsorption of phenolic compounds

The effect of contact time (15 to 90 min) on the adsorption of phenolic compounds using nanosilica and sodium silicate was investigated. The amount of adsorbed phenols reached 1024.9 mg/g after just 15 minutes using 0.5% nanosilica at 200 rpm. In contrast, when using sodium silicate as the adsorbent, the amount adsorbed reached 130.68 mg/g after 52.5 minutes with 2% adsorbent at 100 rpm. As shown in Table II, the maximum percentage removal for nanosilica was observed within the first 15 minutes. This rapid efficiency can be attributed to the small size of phenolic molecules, which allows for easy diffusion into vacant adsorption sites. The high availability of empty surface sites at the beginning of the experiment significantly increases the initial adsorption rate. Subsequently, the occupation of vacant sites slows due to repulsive forces between adsorbed and unabsorbed molecules.[14]

A comparative analysis of equilibrium times with diverse adsorbents including olive pomace for 24 hours, activated carbon for 4 hours, and natural Ghassoul clay for 2 hours demonstrates that nanosilica achieves adsorption equilibrium for OMW constituents significantly faster. This enhanced kinetic performance suggests superior mass transfer properties and more accessible active sites in the nanostructured material.[31,33]

Effect of stirring speed (rpm) on adsorption performance

The influence of stirring speed (rpm) on adsorption performance was investigated for both adsorbents. When using nanosilica, increasing the rotational speed from 100 to 300 rpm generally enhanced solution mixing and improved contact between the adsorbent and phenolic compounds, thereby promoting removal efficiency. The experimental data reveal distinct trends: at 200 rpm, removal efficiency ranged between 86.08% and 89.97%. At 300 rpm, efficiency only marginally improved to 87.06%–88.93%, suggesting that exceeding 200 rpm did not significantly enhance performance, likely due to kinetic saturation. At 100 rpm, efficiency was comparatively lower (85.00%–88.29%) due to insufficient mixing, which reduced interactions. The optimal agitation speed for maximizing

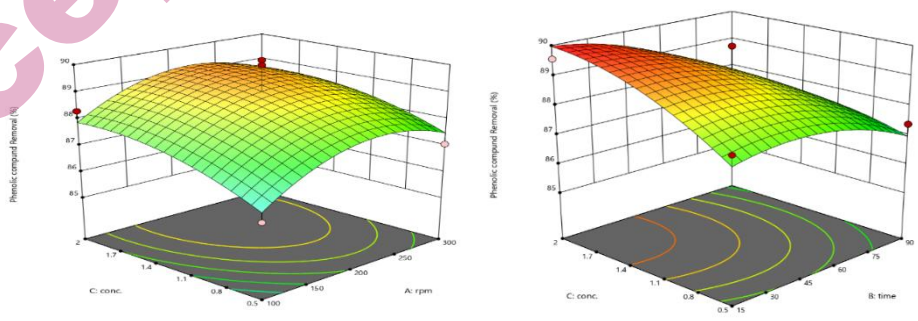
Accepted manuscript

removal efficiency was 200 rpm, as higher speeds yielded diminishing returns while lower speeds resulted in suboptimal mixing. This observation aligns with the principle that sufficient turbulence enhances diffusion, whereas excessive agitation provides no additional benefit once equilibrium is approached. On the other hand, when using sodium silicate, the experimental data showed different trends. At 300 rpm, phenolic compound removal efficiency ranged between 44.12% and 72.12%. When the speed was decreased to 200 rpm, the efficiency ranged from 43.25% to 66.56%. Finally, at 100 rpm, efficiency was comparatively lower (44.12%–55.48%) due to insufficient mixing, which reduced interactions between sodium silicate and the phenolic compounds.

Maximum phenolic compound removal efficiencies obtained in this study were compared with various agricultural waste-derived adsorbents reported in recent literature TableV.

Table V: Comparison of phenolic removal efficiencies by different bio-adsorbents.

Adsorbents	Dose / conditions	Removal Efficiency %	Reference
Sugarcane bagasse	60 min at 60 °C and pH of 12	60 %	[34]
Rice husk	Thermally activated rice husk	36-64%	[35]
Rice husk	Chemically activated rice husk	28%	[35]
Wheat husks	Biochar dose 0.5, pH 4,1h.	84%	[36]
Rice husk	Extracted nanosilica	89.979%	This study
Rice husk	Extracted sodium silicate	72.45%	This study



(a) (b)

Fig. 9. Effect of interaction between adsorbent dosage, time and rpm on phenolic compound removal %. (a) nanosilica concentration interaction with rpm, (b) nanosilica concentration interaction with time, (c) sodium silicate concentration interaction with rpm, (d) sodium silicate concentration interaction with time.

Accepted manuscript

Adsorption isotherm

The adsorption equilibrium data were evaluated by correlation them with Langmuir and Freundlich isotherm models. Adsorption phenomena are described by two main models: the Langmuir model, where monolayer adsorption on homogeneous surface is described, and the Freundlich model, where adsorption in heterogenous surface (with exponentially decreasing adsorption energy) is assumed. The isotherms are shown in Fig. 10, and the parameters extracted from these models are summarized in Table VI.

Langmuir model, with near-perfect correlation coefficients ($R^2 \approx 0.999$ for both adsorbents), indicates that monolayer adsorption is the dominant process on homogeneous surfaces. The exceptionally high maximum monolayer adsorption capacity (q_m) of nanosilica (1878.751 mg/g), which is an order of enormity greater than that of sodium silicate (126.47 mg/g), clearly establishes its superior efficacy. Furthermore, the lower K_l value for nanosilica (0.296 L/mg) compared to sodium silicate (0.494 L/mg) suggests a lower affinity for the adsorbate at low concentrations, though this is secondary to the dominant effect of its high q_m value.

While Freundlich model also showed a strong correlation, particularly for nanosilica ($R^2 = 0.9994$), its slightly lower fit compared to Langmuir model reinforces the interpretation of monolayer coverage. Freundlich intensity parameters (1/n) for both materials were less than 1 (0.250 and 0.289, respectively), confirming that adsorption is a favorable process. The value for nanosilica, being closer to zero, indicates a more heterogeneous surface energy distribution and a stronger tendency toward chemisorption compared to sodium silicate.[37]

The Dubinin–Radushkevich (D–R) model was employed to determine the underlying adsorption mechanism and compare the binding properties of the two adsorbents. The plots of ln q_e versus ε^2 yielded high correlation coefficients for both nanosilica ($R^2 = 0.9914$) and sodium silicate ($R^2 = 0.9803$), Fig. 10. From the respective slopes, the activity coefficients β were determined to be 0.0213 mol^2/J^2 for nanosilica and 0.1136 mol^2/J^2 for sodium silicate. Furthermore, the theoretical maximum adsorption capacities (q_m) predicted by the D-R model were 10.83 mg/g and 199.16 mg/g for nanosilica and sodium silicate, respectively.

The mean free energy of adsorption (E) was calculated to be 4.845 J/mol for nanosilica and 2.098 J/mol for sodium silicate. Since the magnitude of E for both synthesized materials is strictly below 8 kJ/mol, it conclusively indicates that the removal of phenolic compounds from the olive mill wastewater is governed by a physisorption mechanism. This suggests that the adsorption process is primarily driven by physical forces, such as van der Waals interactions, hydrogen bonding, and electrostatic attraction, rather than chemical ion-exchange.[38]

Accepted manuscript

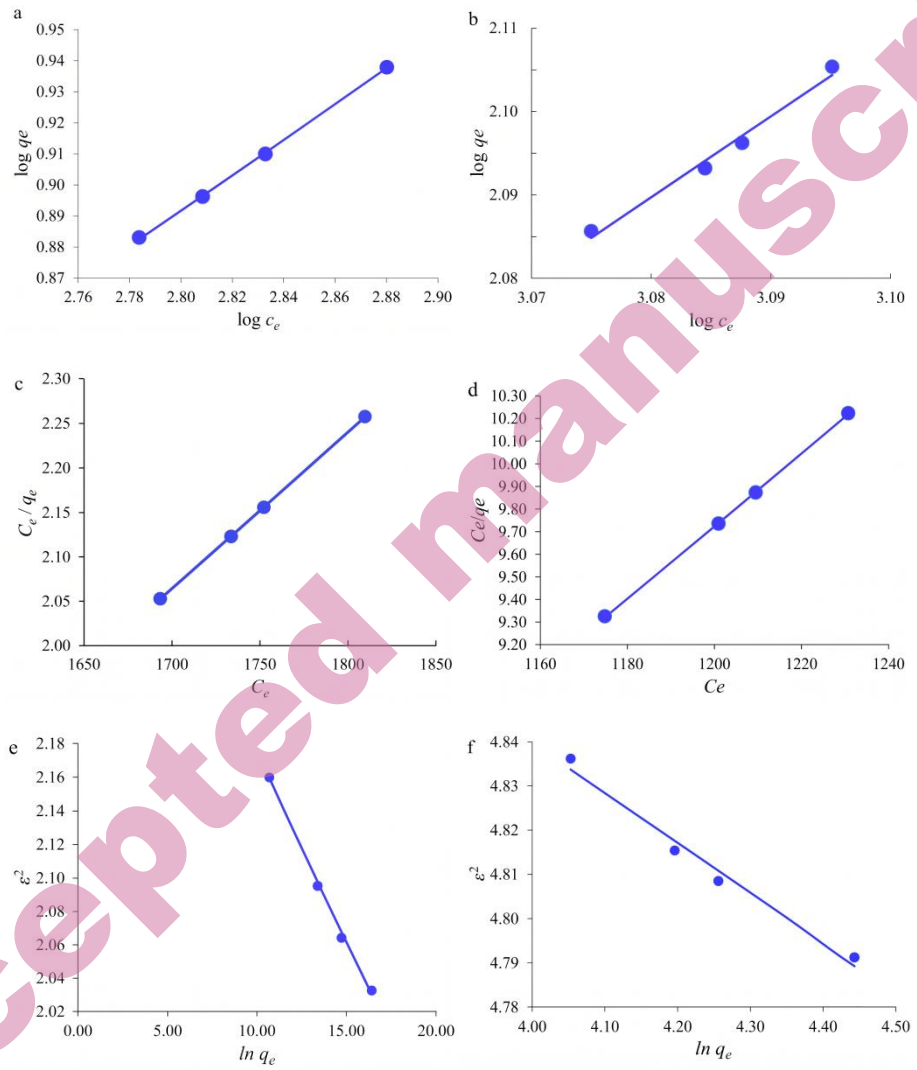


Fig.10. linear regression of OMW phenolic compounds adsorption isotherm on nanosilica and sodium silicate: (a) Freundlich nanosilica , (b) Freundlich sodiumsilicate, (c) Langumuir nanosilica, (d) Langumuir sodium silicate, (e) Dubinin–Radushkevich nanosilica and (f) Dubinin–Radushkevich sodium silicate.

Adsorption kinetic

The experimental results were explained using various kinetic models including the parameters governing the adsorption process. Two kinetic models were employed: pseudo first order pseudo and second order. The most suitable model was selected based on the correlation coefficient R^2, where the value closer to 1 indicates the best fit for describing the adsorption process, Table VII.

Accepted manuscript

Table VI. Linear equation of isotherm models.

model	parameter	nanosilica	sodium silicate
Langmuir	qm, mg/g	1878.75	126.47
	K_L, mg/L	0.2958	0.4943
	R^2	0.9999	0.9998
Freundlich	K_F , mg/g	0.5708	0.9678
	1/n	0.25000	0.2894
	R^2	0.9994	0.9844
Dubinin–Radushkevich	qm, mg/g	10.835	199.16
	β, mol^2/J^2	0.0213	0.1136
	E, kJ/mol	0.0048	0.0021
	R^2	0.9914	0.9803

Figure 11 exhibits the logarithmic plots of (q_e - q_t) as a function of time, from which the slope and intercept were used to calculate the pseudo first order constant K_1 and q_e. According to Table VI, the correlation coefficients (R^2) for this model were 0.9864 for nanosilica and 0.9858 for sodium silicate. However, the calculated q_e values for both adsorbents deviated significantly from the experimentally observed q_e, indicating that the pseudo first order model does not adequately characterize the adsorption kinetics of organic matter from OMW onto these adsorbents.[31]

The pseudo second order kinetics is expressed in a linear form by equation (9). The values of q_e and k_2 can be acquired from the slope and intercept of the plot of t/q_t versus time. The parameters derived from this kinetic model is presented in Table V. The correction coefficient R^2 were 0.9943 and 0.9998 for nanosilica and sodium silicate, respectively. Furthermore, the calculated q_e values for both adsorbents were very close to the experimental values. Therefore, the pseudo second order model provides a better description of the adsorption process of OMW onto nanosilica and sodium silicate.[31]

To further elucidate the diffusion mechanisms and compare the kinetic behaviors of the two adsorbents, the experimental data were fitted to the Weber-Morris intra-particle diffusion model. The high correlation coefficients obtained for both nanosilica (R^2 = 0.9946) and sodium silicate (R^2= 0.9914) indicate the suitability of this model for describing the process. The intra-particle diffusion rate constant (K_{id}) for nanosilica was found to be 18.879 mg/(g.$min^{0.5}$), which is significantly higher than that of sodium silicate 0.994 mg/(g.$min^{0.5}$). This substantial difference suggests a much faster diffusion rate of phenolic compounds into the internal porous structure of the nanosilica.[18]

Accepted manuscript

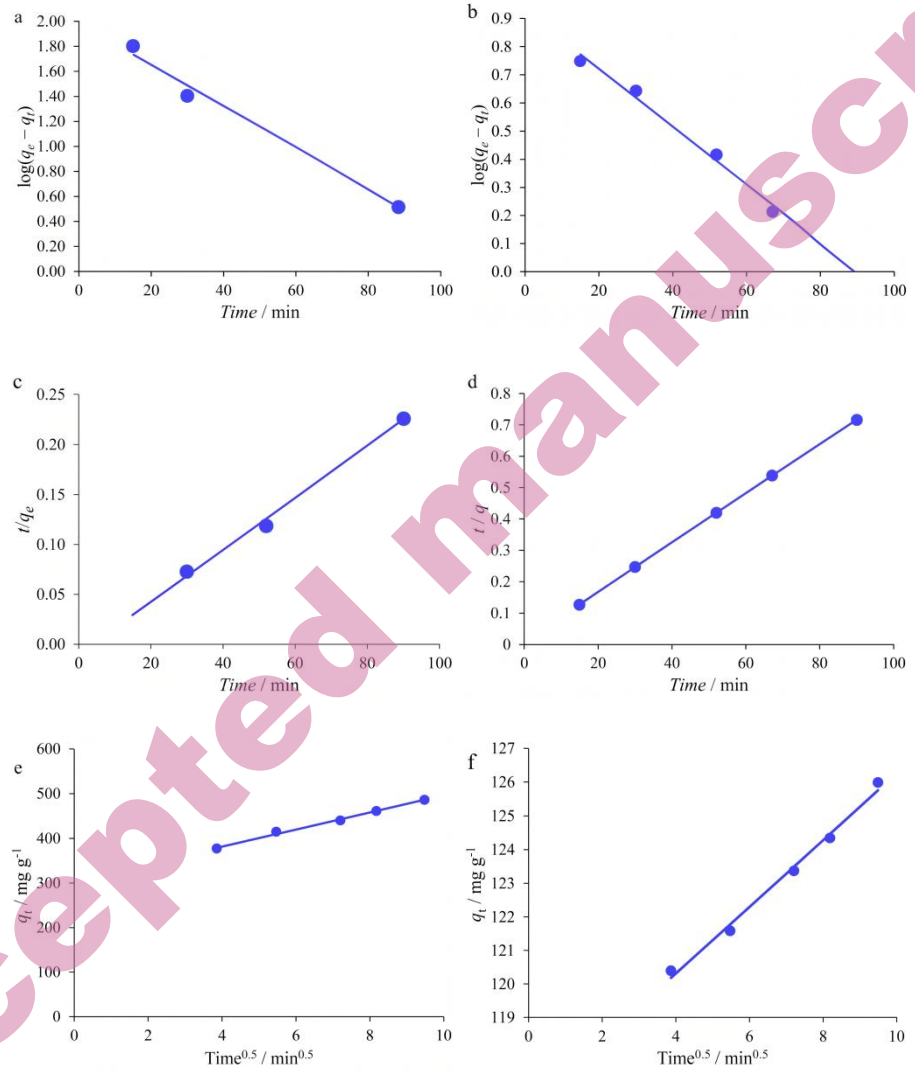


Fig. 11. Kinetic parameters on pseudo first and second orders models for phenolic compounds adsorption on nanosilica and sodium silicate: (a) pseudo first order for nanosilica , (b) pseudo first order for sodium silicate, (c) pseudo second order for nanosilica, (d) pseudo second order for sodium silicate, (e) Weber-Morris model for nanosilica and (f) Weber-Morris model for sodium silicate.

Furthermore, the boundary layer thickness constant (C) was calculated to be 306.56 mg/g for nanosilica and 116.33 mg/g for sodium silicate. Crucially, the plots for both materials did not pass through the origin ($C \neq 0$), demonstrating that intra-particle diffusion is not the sole rate-limiting step in either case. Instead, the

Accepted manuscript

non-zero intercepts confirm that the overall adsorption of phenols from the olive mill wastewater onto these rice husk-derived materials is governed by a complex, multi-step mechanism involving both external mass transfer (film diffusion) across the boundary layer and subsequent intra-particle diffusion.[38 39 40]

Table VII: Parameters of pseudo first order, pseudo second order and Weber-Morris models for phenolic compounds adsorption on nanosilica and sodium silicate.

model	parameters	nanosilica	sodium silicate
pseudo 1st order	qe exp, mg/g	440	125
	qe cal, mg/g	95.9800	8.4178
	K1, min-1	0.0380	0.0235
	R2	0.9864	0.9858
pseudo 2nd order	qe exp, mg/g	440	125
	qe cal, mg/g	384.6154	126.5823
	K2, g/mg. min	0.0007	0.0065
	R2	0.9943	0.9998
Weber-Morris	Kid, mg/g.min0.5	18.879	0.994
	C, mg/g	306.56	116.33
	R2	0.9946	0.9914

Thermodynamic studies

The thermodynamic parameters Gibbs free energy (ΔG°), enthalpy (ΔHº), and entropy (ΔSº) changes were evaluated at temperatures of 308.15, 318.15, and 328.15 K to fully characterize the energetic nature of the adsorption process, fig. 12. Across all tested temperatures (table VIII), both nanosilica and sodium silicate exhibited negative ΔGº values, confirming that the sequestration of phenolic compounds from the aqueous phase is a spontaneous and thermodynamically favorable process. The relatively low magnitude of these free energy changes (ranging from -0.947 to -1.853 kJ/mol) further corroborates the isotherm findings, firmly establishing that the predominant binding mechanism is physisorption rather than chemisorption.[18]

Despite both materials demonstrating spontaneous uptake, their thermal behaviors are The adsorption onto nanosilica is characterized by a negative enthalpy change (ΔHº= -0.1178 kJ/mol), indicating an exothermic process where energy is released upon binding, making lower temperatures slightly more favorable for adsorption. Furthermore, nanosilica exhibits a negative entropy change (ΔSº= -0.7017 J/mol.K), signifying a decrease in randomness at the solid-liquid interface as the phenolic molecules transition from a mobile liquid phase to a highly ordered state on the silica surface.

Conversely, the interaction with sodium silicate is inherently endothermic, evidenced by a positive enthalpy change (ΔHº= 9.580 kJ/mol), which suggests that heat input facilitates the adsorbate-adsorbent interactions, leading to a more negative (ΔGº) at higher temperatures. Notably, sodium silicate displays a significantly positive entropy change (ΔSº= 34.95 J/mol.K). This increase in

Accepted manuscript

interfacial randomness is highly indicative of an entropy-driven process, likely resulting from the substantial structural displacement and release of physically adsorbed water molecules from the surface of the sodium silicate as the bulky phenolic compounds are adsorbed, thereby increasing the overall degrees of freedom in the system.[18,40]

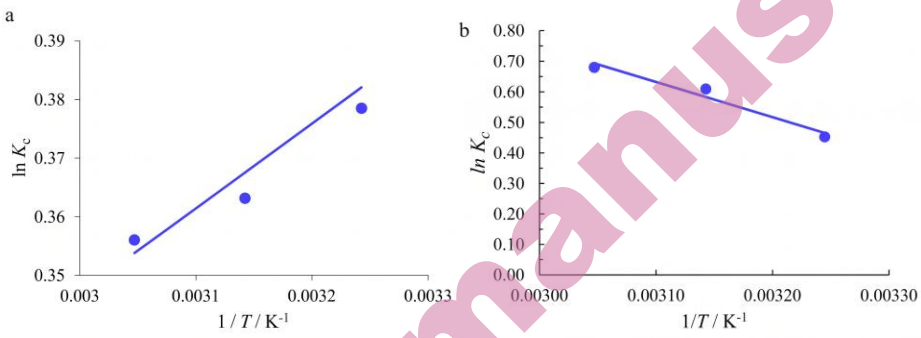


Fig. 12. Van't Hoff plots for the adsorption of phenolic compounds onto (a) nanosilica and (b) sodium silicate.

Table VIII: Thermodynamic parameters for phenolic compounds adsorption on nanosilica and sodium silicate.

Adsorbent	T / K	ln Kc	ΔG° / kJ/mol	ΔH° / kJ/mol	ΔS° / J/mol.K
nanosilica	308.15	0.379055	-0.971	-0.1178	-0.7017
	318.15	0.358191	-0.947		
	328.15	0.351071	-0.958		
sodium silicate	308.15	0.452199	-1.159	9.5802	34.9529
	318.15	0.608168	-1.608		
	328.15	0.679289	-1.853		

Adsorption mechanism of phenolic compounds

The adsorption of phenolic compounds onto the rice husk-derived nanosilica and sodium silicate is governed by a synergistic, multi-step physisorption mechanism. Spectroscopic and isothermal evidence indicates that the interactions are primarily driven by hydrogen bonding between the hydroxyl and aromatic moieties of the phenolic molecules and the isolated surface silanol (Si–OH) groups of the adsorbents. Additionally, weak physical forces specifically van der Waals interactions and dipole-dipole attractions facilitate surface complexation, a conclusion strictly supported by the low mean free energy of adsorption ($E < 8$ kJ/mol) derived from the Dubinin–Radushkevich model. Kinetically, the sequestration process proceeds through a sequential transport mechanism: initial external mass transfer (film diffusion) of the phenolics across the hydrodynamic boundary layer, followed by intra-particle diffusion into the internal porous network of the silicates, culminating in physical immobilization at the active binding sites (Fig. 13).[18,38]

Accepted manuscript

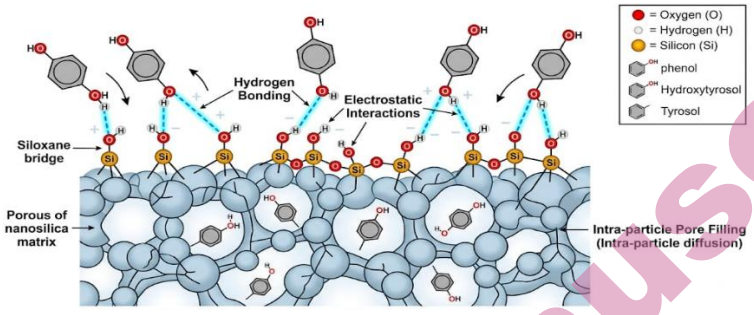


Figure 13. Schematic illustration of the proposed adsorption mechanism of phenolic compounds from olive mill wastewater onto rice husk-derived nanosilica and sodium silicate.

CONCLUSION

This study demonstrates the superior performance of rice husk-derived nanosilica over sodium silicate for the adsorptive removal phenolic compounds from olive mill wastewater OMW. Under optimized conditions, a nanosilica dosage of 0.5% achieved a high removal efficiency of 89.979% and a remarkable adsorption capacity of 1024.9 mg/g. A key advantage of nanosilica is its rapid adsorption kinetics, reaching equilibrium within just 15 minutes, which signifies superior mass transfer properties compared to conventional adsorbents. The process was further optimized at a stirring speed of 200 rpm. In comparison, sodium silicate yielded a capacity of 130.68 mg/g and 72.45% removal (2% concentration, 52.5 min, 300 rpm). Collectively, these findings establish nanosilica as a highly efficient and kinetically favorable adsorbent, offering a rapid, effective, and scalable solution for OMW treatment. Its high capacity and fast equilibrium kinetics demonstrate significant potential for reducing reactor volume and treatment time in industrial wastewater remediation applications. Mechanistic investigations utilizing the Dubinin–Radushkevich isotherm and thermodynamic modeling conclusively proved that the sequestration of phenolics by both materials is governed by a spontaneous physisorption process, driven predominantly by hydrogen bonding, van der Waals forces, and electrostatic interactions. Despite sharing a fundamental physisorption mechanism, the two adsorbents exhibited distinct kinetic and thermodynamic behaviors. Kinetic modeling via the Weber-Morris equation established that adsorption is controlled by a multi-step sequence involving both external film diffusion and intra-particle diffusion. Notably, nanosilica demonstrated a remarkably superior intra-particle diffusion rate kid = 18.879 mg/g.min$^{0.5}$ compared to sodium silicate 0.994 mg/g.min$^{0.5}$, facilitating more rapid adsorbate transport into its internal porous network. Thermodynamically, phenolic uptake by nanosilica was exothermic and enthalpy-driven $\Delta H° < 0$), whereas adsorption onto sodium silicate was endothermic and heavily entropy-driven $\Delta S° > 0$), likely due to the extensive displacement of

Accepted manuscript

interfacial water molecules. Ultimately, both rice husk-derived materials proved to be highly viable, sustainable alternatives to conventional commercial adsorbents.

While this study establishes a strong theoretical and mechanistic foundation in batch systems, future research should focus on the transition toward industrial scale-up. Specifically, comprehensive desorption and regeneration studies must be conducted to assess the multi-cycle reusability and long-term lifecycle costs of the adsorbents, further cementing their role in a circular economy. Finally, investigating the competitive adsorption dynamics in raw, untreated OMW which contains a complex matrix of competing organic and inorganic pollutants will be critical for optimizing these biogenic materials for full-scale commercial wastewater treatment facilities.

И З В О Д

ОДРЖИВО ПРЕЧИШЋАВАЊЕ ОТПАДНИХ ВОДА ИЗ ПРОИЗВОДЊЕ МАСЛИНОВОГ УЉА: ПОРЕЂЕЊЕ ЕФИКАСНОСТИ УКЛАЊАЊА ФЕНОЛНИХ ЈЕДИЊЕЊА ПРИМЕНОМ НАНО СИЛИЦИЈУМ-ДИОКСИДА И НАТРИЈУМ-СИЛИКАТА ДОБИЈЕНИХ ИЗ ПИРИНЧАНЕ ЉУСКЕ

MARWA M. HELMY* И AMIRA S. EL MAHROUKY

Food Engineering and Packaging Department, Food Technology Research Institute, Agricultural Research Center, Giza, Egypt.

У овом истраживању испитана је могућност пречишћавања отпадних вода из производње маслиновог уља применом нано силицијум-диоксида и натријум-силиката екстрахованих из пиринчане љуске. Ови одрживи адсорбенти окарактерисани су применом FTIR спектроскопије, UV-VIS спектроскопије и анализе величине честица, а затим је испитана њихова ефикасност у уклањању фенолних једињења. За оптимизацију параметара шаржне адсорпције, укључујући концентрацију адсорбента, време мешања и број обртаја, примењена је методологија одзивних површина. Нано силицијум-диоксид је показао супериорне адсорпционе карактеристике, остварујући максимални адсорпциони капацитет од 1024,9 mg/g и ефикасност уклањања од 89,979% при оптималним условима (концентрација адсорбента 0,5%, време 15 минута и број обртаја 200 rpm). Насупрот томе, применом натријум-силиката постигнут је адсорпциони капацитет од 130,68 mg/g и ефикасност уклањања од 72,45% при следећим оптималним условима: концентрација адсорбента 2%, време 52,5 минута и број обртаја 300 rpm. Поред тога, за описивање адсорпционих механизама примењени су кинетички модели и модели адсорпционих изотерми. Испитивање механизма адсорпције применом Weber-Morris модела показало је да се адсорпциони процес одвија кроз више узастопних фаза, које обухватају дифузију кроз гранични филм и дифузију унутар честица, при чему је нано силицијум-диоксид показао знатно већу брзину унутрашње дифузије (K_{id} = 18,879 mg g^{-1} $min^{-0.5}$). Такође, вредности термодинамичких параметара ($\Delta G < 0$), као и Dubinin–Radushkevich адсорпциона изотерма (E < 8 kJ/mol), недвосмислено су указале на то да се процес уклањања полутаната одвија путем спонтане физичке адсорпције (физисорпције). Добијени резултати потврђују потенцијал материјала добијених из пиринчане љуске као ефикасних и еколошки прихватљивих адсорбената за пречишћавање отпадних вода из производње маслиновог уља.

(Примљено 23. јануара; ревидирано 3. марта; прихваћено 13. новембра 2026.)

Accepted manuscript

REFERENCES

1. S. Ijaz, A. Kausar, M. Iqbal, N. El Messaoudi, Y. Miyah, S. Knani, B. Graba, *J. Water Process Eng.* **71** (2025) 107187 (https://doi.org/10.1016/j.jwpe.2025.107187)
2. A. Jamrah, T. M. Al-Zghoul, M. M. Darwish, *Case Stud. Chem. Environ. Eng.* **8** (2023) 100493 (https://doi.org/10.1016/j.cscee.2023.100493)
3. K. O. Rocha, F. Brandão, C. Mendes, M. G. V. S. Carvalho, P. Mazierski, A. Zaleska-Medynska, J. Gomes, R. C. Martins, E. Domingues, *Catal. Today* **432** (2024) 114618 (https://doi.org/10.1016/j.cattod.2024.114618)
4. L. Al-Hmoud, B. Al-Saida, A. Sandouqa, *Jordanian J. Eng. Chem. Ind.* **3** (2020) 91–106 (https://doi.org/10.48103/jjeci3112020)
5. M. O. J. Azzam, *J. Environ. Chem. Eng.* **6** (2018) 2126–2136 (https://doi.org/10.1016/j.jece.2018.03.009)
6. M. O. J. Azzam, S. A. Hazaimeh, *Process Saf. Environ. Prot.* **148** (2021) 495–523 (https://doi.org/10.1016/j.psep.2020.10.030)
7. A. Faggiano, M. De Carluccio, A. Fiorentino, M. Ricciardi, R. Cucciniello, A. Proto, L. Rizzo, *Sep. Purif. Technol.* **305** (2023) 122525 (https://doi.org/10.1016/j.seppur.2022.122525)
8. J. R. Balbinoti, R. E. dos Santos Junior, L. B. F. de Sousa, F. de Jesus Bassetti, T. C. V. Balbinoti, L. M. de Matos Jorge, R. M. M. Jorge, *J. Water Process Eng.* **52** (2023) 103525 (https://doi.org/10.1016/j.jwpe.2023.103525)
9. S. M. T. Al-Abboodi, E. J. A. Al-Shaibani, E. A. Alrubai, *IOP Conf. Ser.: Mater. Sci. Eng.* **978** (2020) 012031 (https://doi.org/10.1088/1757-899x/978/1/012031)
10. M. Sorour, M. Helmy, A. S. EL Mahrouky, I. I. Ahmed, *Food Technol. Res. J.* **2** (2023) 68–72 (https://doi.org/10.21608/ftrj.2023.329291)
11. X. Liu, Z. Li, H. Chen, L. Yang, Y. Tian, Z. Wang, *Res. Chem. Intermed.* **42** (2016) 3887–3903 (https://doi.org/10.1007/s11164-015-2251-7)
12. Y. Cardona, S. A. Korili, A. Gil, *Chem. Eng. J.* **425** (2021) 130708 (https://doi.org/10.1016/j.cej.2021.130708)
13. A. Yangui, M. Abderrabba, A. Sayari, *J. Taiwan Inst. Chem. Eng.* **70** (2017) 111–118 (https://doi.org/10.1016/j.jtice.2016.10.053)
14. F. Elayadi, W. Boumya, M. Achak, Y. Chhiti, F. E. M. Alaoui, N. Barka, C. El Adlouni, *Environ. Challenges* **4** (2021) 100184 (https://doi.org/10.1016/j.envc.2021.100184)
15. L. Dolatyari, M. R. Yaftian, S. Rostamnia, *J. Environ. Manage.* **169** (2016) 8–17 (https://doi.org/10.1016/j.jenvman.2015.12.005)
16. H. S. Titah, I. F. Purwanti, B. V. Tangahu, S. B. Kurniawan, M. F. Imron, S. R. S. Abdullah, N. Ismail, *J. Environ. Manage.* **238** (2019) 194–200 (https://doi.org/10.1016/j.jenvman.2019.03.011)
17. Y. Zhou, Y. Li, D. Liu, X. Wang, D. Liu, L. Xu, *Colloids Surf. A Physicochem. Eng. Asp.* **607** (2020) 125422 (https://doi.org/10.1016/j.colsurfa.2020.125422)
18. M. S. Slimani, M. Aazza, H. Ahlafi, A. El-Kordy, H. Barkouch, M. Amar, O. T. Alaoui, M. Hamidi, *J. Mol. Liq.* **457** (2026) 129704 (https://doi.org/10.1016/j.molliq.2026.129704)
19. E. Rafiee, S. Shahebrahimi, M. Feyzi, M. Shaterzadeh, *Int. Nano Lett.* **2** (2012) 29 (https://doi.org/10.1186/2228-5326-2-29)
20. V. B. Carmona, R. M. Oliveira, W. T. L. Silva, L. H. C. Mattoso, J. M. Marconcini, *Ind. Crops Prod.* **43** (2013) 291–296 (https://doi.org/10.1016/j.indcrop.2012.06.050)

Accepted manuscript

21. A. Jyoti, R. K. Singh, N. Kumar, A. K. Aman, M. Kar, *Mater. Sci. Eng. B* **263** (2021) 114871 (https://doi.org/10.1016/j.mseb.2020.114871)
22. F. M. Mohamed, K. A. Alfalous, *Egypt. J. Aquat. Res.* **46** (2020) 131–136 (https://doi.org/10.1016/j.ejar.2020.03.004)
23. A. I. Biradar, P. D. Sarvalkar, S. B. Teli, C. A. Pawar, P. S. Patil, N. R. Prasad, *Mater. Today Proc.* **43** (2021) 2832–2838 (https://doi.org/10.1016/j.matpr.2020.11.946)
24. M. Sadeghi, M. Dorodian, M. Rezaei, *J. Adv. Chem.* **6** (2013) 917–922
25. A. Eslami, M. Mehralian, Z. G. Chegini, M. Khashij, *Desalin. Water Treat.* **108** (2018) 345–352 (https://doi.org/10.5004/dwt.2018.21966)
26. Y. Dehmani, L. Sellaoui, Y. Alghamdi, J. Lainé, M. Badawi, A. Amhoud, A. Bonilla-Petriciolet, T. Lamhasni, S. Abouarnadasse, *J. Mol. Liq.* **312** (2020) 113383 (https://doi.org/10.1016/j.molliq.2020.113383)
27. G. La Scalia, R. Micale, L. Cannizzaro, F. P. Marra, *J. Clean. Prod.* **142** (2017) 3782–3788 (https://doi.org/10.1016/j.jclepro.2016.10.086)
28. A. F. Al Bawab, M. A. Abu-Dalo, H. Kanaan, N. Al-Rawashdeh, F. Odeh, *Water Sci. Technol.* **91** (2025) 567–580 (https://doi.org/10.2166/wst.2025.007)
29. L. Papaoikonomou, K. Labanaris, K. Kaderides, A. M. Goula, *Environ. Sci. Pollut. Res.* **28** (2021) 24230–24244 (https://doi.org/10.1007/s11356-019-07277-2)
30. D. Bouazzi, A. Mehri, K. Kaaroud, H. Touati, F. Karouia, J. M. Clacens, A. Laghzizil, B. Badraoui, *Colloids Surf. A Physicochem. Eng. Asp.* **666** (2023) 131366 (https://doi.org/10.1016/j.colsurfa.2023.131366)
31. M. Ammari, M. Zerrouk, I. Zoufri, Y. El-Byari, A. Mazrha, F. E. Mrizak, M. Merzouki, *Sci. African* **27** (2025) e02612 (https://doi.org/10.1016/j.sciaf.2025.e02612)
32. M. Ververi, A. M. Goula, *Chem. Eng. Process. Intensif.* **138** (2019) 86–96 (https://doi.org/10.1016/j.cep.2019.03.010)
33. G. Enaime, W. El Bouaidi, M. Louarrat, A. Baçaoui, A. Yaacoubi, M. Loudiki, M. Wichern, M. Lübken, *Biomass Convers. Biorefinery* **15** (2025) 4153–4165 (https://doi.org/10.1007/s13399-023-05261-y)
34. M. B. Bahrodin, N. S. Zaidi, A. Kadier, N. Hussein, A. Syafiuddin, R. Boopathy, *Appl. Sci.* **12** (2022) 7972 (https://doi.org/10.3390/app12167972)
35. A. Kumari, M. Yadav, N. Kumar, *Bull. Pure Appl. Sci.* **42** (2023) 101–105 (https://doi.org/10.48165/bpas.2023.42c.2.6)
36. M. F. Al Rawi, G. Y. Al Kindi, J. K. Al Refaae, T. A. Hussain, H. A. Al-Haidri, *IOP Conf. Ser. Earth Environ. Sci.* **1222** (2023) (https://doi.org/10.1088/1755-1315/1222/1/012012)
37. M. A. Masmoudi, N. Abid, F. Feki, F. Karray, M. Chamkha, S. Sayadi, *Euro-Mediterranean J. Environ. Integr.* **9** (2024) 621–635 (https://doi.org/10.1007/s41207-024-00464-9)
38. Y. Zhou, Y. Li, D. Liu, D. Liu, L. Xu, C. Liu, *Colloids Surf. A Physicochem. Eng. Asp.* **627** (2021) 127145 (https://doi.org/10.1016/j.colsurfa.2021.127145)
39. S. Allaoui, *RHAZES Green Appl. Chem.* **6** (2019) 40–46 (https://doi.org/10.1155/2020/7293189)
40. S. Allaoui, M. N. Bennani, H. Ziyat, O. Qabaqous, N. Tijani, N. Ittobane, G. Hodaifa, *Heliyon* **7** (2021) e07525 (https://doi.org/10.1016/j.heliyon.2021.e07525).

Accepted manuscript